




# Subnanosecond Marx Generators for Picosecond Gain-Switched Laser Diodes

Fuyi Cao, Dongxin Jiang, Yuejun Liu, Yunpeng Tian, Xu Ran, Yisu Long, Takashi Ito, Xiaobo Hu , Guoen Weng , Hidefumi Akiyama, and Shaoqiang Chen 

**Abstract**—High precision time-of-flight based light detection and ranging (LiDAR) system needs compact ultrafast pulsed lasers, such as gain-switched semiconductor laser diodes, which have the advantages of low cost, small size, and mass-producible, for short pulse generation, and are of great interest in many other fields, where low-cost high-voltage electrical pulse generators are in demand to directly modulate laser diodes for practical applications. Here, we presented a low-cost subnanosecond electrical pulse generator based on avalanche transistors, with output electrical pulses having a maximum peak voltage of approximately 25 V and a minimum pulse width of approximately 450 ps, depending on load impedance. We applied the electrical pulses on a gallium nitride (GaN)-based blue-violet laser diode, and demonstrated typical gain-switching characteristics of the laser diode. The minimum pulse width of the first spike of the gain-switched optical pulses was as short as 23 ps. In addition, we constructed a field-programmable gate array (FPGA)-triggered Marx generator with programmable frequency, and demonstrated its practicability in characterizing the transient gain-switching properties of laser diodes with a streak camera. These results should be of significant interest for both industrial applications and scientific research.

**Index Terms**—Avalanche transistor, electric circuit, gain switch, laser diode, picosecond, pulse generation.

## I. INTRODUCTION

**I**N OUR previous studies, we have demonstrated that even with subnanosecond electrical pulses, optical pulses with several-picosecond duration can be generated from gain-switched semiconductor lasers combined with a low-cost

spectral-filtering technique [1], [2], which allows the use of low-cost subnanosecond electrical pulses for short optical pulse generation. Therefore, developing subnanosecond electrical pulses with even lower cost and higher output voltage are of great significance for short pulse generation in gain-switched semiconductor lasers.

Avalanche transistor having high nonlinear gain is known to be useful in electrical pulse generation since its invention [3], [4], and is still attracting interests in both fundamental research and practical applications [5], [6], [7], [8]. Generally, an avalanche transistor-based Marx circuit can generate electrical pulses in the subnanosecond range [9], [10], which have been widely used in radar, medical treatment, etc. [1], [2], [3], [4], [5], [6], [7], [8], [9], [10], [11], [12]. Recently, the generation of electrical pulses with a peak voltage as high as 2 kV and a rise time as short as 200 ps has been reported, through selecting proper avalanche transistors and reducing the parasitic inductance and capacitance of the printed circuit board (PCB) [13], which clearly demonstrated the strong ability of avalanche transistors in high-voltage pulse generation. With proper design, the avalanche-transistor-based electrical pulse generators should also be suitable for gain-switched semiconductor laser diodes, however, related study has barely been reported thus far [14], [15]. J. Vanderwall et al. [14] used an avalanche transistor for three-stacked laser diodes and generated 120-ps optical pulses, while B. Lanz et al. [15] used a GaAs-based fast avalanche transistor to pump an 850-nm laser diode, which demonstrated the gain-switching characteristics of the laser diode, and generated 40–70 ps high-power optical pulses. Compared to the high-voltage avalanche transistors used in several of the above papers, we used a low-voltage avalanche transistor for the circuit design, which produces pulse currents at much lower breakdown voltages and is more suitable for gain-switching semiconductor lasers.

In this article, we demonstrated that even with the present silicon-based avalanche transistors, semiconductor laser diodes can be well driven, and the gain-switching characteristics of laser diodes were systematically investigated. First, we used low-cost avalanche transistors to construct a subnanosecond electrical pulse generator with a maximum peak voltage of 25 V and a minimum pulse width of 450 ps, depending on the load impedance. Next, we applied the output electrical pulses of the pulse generator onto a GaN-based blue laser diode for the gain-switching operation, and short laser pulses with a duration as short as 23 ps were generated. We then constructed

Manuscript received 3 October 2023; revised 25 November 2023; accepted 10 December 2023. Date of publication 13 December 2023; date of current version 16 January 2024. This work was supported in part by the National Key R&D Program of China under Grant 2022YFF1202604, in part by the National Natural Science Foundation of China under Grant 62274065, in part by the Natural Science Foundation of Chongqing, China under Grant CSTB2023NSCQ-MSX1034, and in part by KAKENHI from the Japan Society for the Promotion of Science under Grant 21H01361. (Corresponding authors: Shaoqiang Chen; Guoen Weng.)

Fuyi Cao, Dongxin Jiang, Yuejun Liu, Yunpeng Tian, Xu Ran, Yisu Long, Xiaobo Hu, and Shaoqiang Chen are with the State Key Laboratory of Precision Spectroscopy, Department of Electronic Engineering, East China Normal University, Shanghai 200241, China (e-mail: sqchen@ee.ecnu.edu.cn).

Guoen Weng is with the State Key Laboratory of Precision Spectroscopy, Department of Electronic Engineering, East China Normal University, Shanghai 200241, China, also with the Chongqing Key Laboratory of Precision Optics, Chongqing Institute of East China Normal University, Chongqing 401120, China, and also with the Shanghai Key Laboratory of Multidimensional Information Processing, East China Normal University, Shanghai 200241, China (e-mail: egweng@ee.ecnu.edu.cn).

Takashi Ito and Hidefumi Akiyama are with the Institute for Solid State Physics, The University of Tokyo, Chiba 277-8581, Japan.

Digital Object Identifier 10.1109/JPHOT.2023.3342450

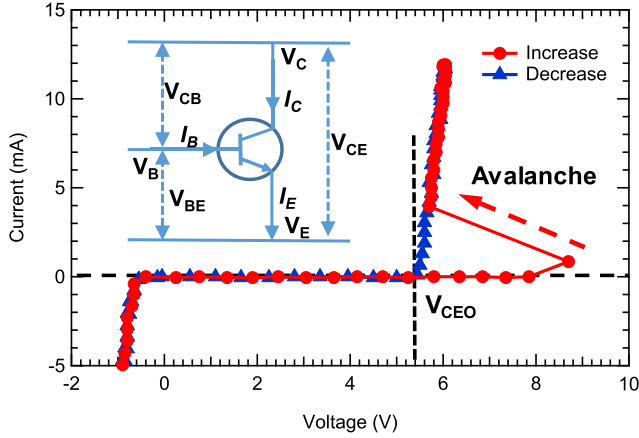


Fig. 1. Current–Voltage ( $I$ – $V$ ) characteristics of the avalanche transistor.

a field-programmable gate array (FPGA)-triggered Marx generator with the proper frequency to match the synchronous scan operation model (synchroscan) of the streak camera, and demonstrated the practicability of the FPGA-triggered Marx generator in characterizing the transient gain-switching properties of laser diodes. Our results are very promising for wide-spread applications, including optical time-of-light (TOF)-based sensing and measurements.

## II. AVALANCHE TRANSISTOR MARX PULSE GENERATORS

Commercial avalanche transistors (BFP450, Infineon) were used in this study. To understand the avalanche-breakdown property of the transistors, the current–voltage ( $I$ – $V$ ) curves of the transistors were first investigated through a curve tracer (Tektronix 370B). Fig. 1 shows the measured  $I$ – $V$  curve of an avalanche transistor. We observed that with an applied voltage of over 8 V between the emitter and collector ( $V_{CE}$ ) of the transistor, avalanche breakdown occurs, resulting in a rapid increase in current and a rapid decrease in voltage (shown as the red dotted line). After the avalanche breakdown, the transistor acts as a resistor (shown as the triangle-marked blue line), and the equivalent resistance is estimated to be approximately 50  $\Omega$  according to the slope of the  $I$ – $V$  curve. The collector current  $I_C$  including the avalanche effects is given by

$$I_C = M(\alpha I_E + I_{CBO}) \quad \text{with } M = 1/[1 - (V_{CE}/BV_{CBO})^m] \quad (1)$$

where  $\alpha$  is the common base current gain,  $M$  is Miller's avalanche multiplication coefficient,  $BV_{CBO}$  is the collector-base breakdown voltage,  $m$  is a constant depending on the material and doping profile of the collector-base junction. From this equation we can see that, with increasing  $V_{CE}$  up to  $BV_{CBO}$ ,  $M$  increases rapidly, resulting in a transient large  $I_C$ , i.e., transient avalanche breakdown. The transient on/off current of the transistor can be used for pulse generation.

Fig. 2 shows a circuit schematic of a designed pulse generator that consists of a single avalanche transistor. The working principle of the circuit can be described as below: Before the trigger pulse arrives, the output of the trigger circuit is in a high-impedance state, when the voltage of the capacitor is equal

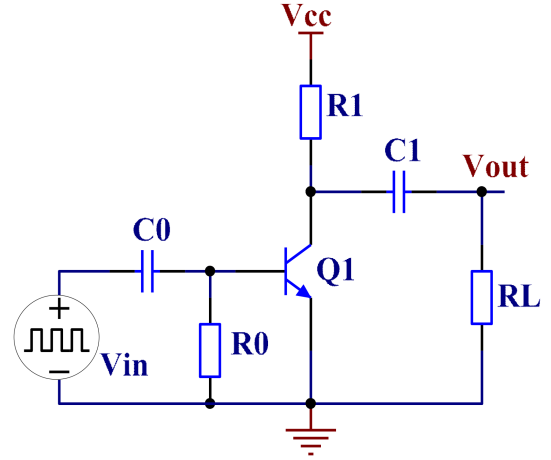


Fig. 2. Circuit schematic of the single avalanche-transistor-based pulse generator.

to the power supply voltage  $V_{CC}$ , i.e.,  $V_{CE} = V_{CC}$ . At this voltage, the transistor collector is reverse biased, the penetration current flowing into the base region is very small, causing a part of the current to flow from the base through the  $R_0$  out to the ground, and the other part of the current to flow through the emitter to the ground. Then, the base current  $I_B < 0$ , the emitter current  $I_E > 0$ , the transistor is in a steady state, and the collector current is very small, which can be considered to be in the cut-off state.

When the trigger pulse arrives, the base negative current decreases and gradually changes to the forward current. When a critical point is reached, the collector current increases rapidly and the transistor is punctured. Capacitor  $C_1$  is rapidly discharged through transistor  $Q_1$ , and a large transient current flows through the load resistor  $RL$ . When the capacitor  $C_1$  discharge has completed and the trigger pulse of the base disappears, transistor  $Q_1$  is turned off and the power supply charges capacitor  $C_1$  again, while waiting for the next trigger pulse to arrive.

The pulse generation mechanism includes the transient avalanche breakdown of the transistor and the discharge of the storage capacitor  $C_1$ . The rise time of the pulse is mainly determined by the switching time of the transistor, while the pulse amplitude and fall time depend on the values of  $V_{CC}$ ,  $C_1$  and  $RL$  [8]. Therefore, the proper selection of the volume of  $C_1$  is very important. As a storage capacitor, the value of  $C_1$  directly affects the number of stored charge in each cycle of the pulse generation, which determines the maximum power of the output pulse. At the same time,  $C_1$  should not be too large, considering the relation between the signal repetition frequency  $f$  and the allowed charging time  $\tau_1$  of the storage capacitor, as in

$$1/f \geq \tau_1 = R_1 \times C_1 \quad (2)$$

The detailed effect of capacitor  $C_1$  on the output pulse was first investigated. A high-speed oscilloscope (Agilent DSA91304A) with a bandwidth of 13 GHz, and a sampling rate of 40 GSa/s were used for this investigation. The DC supply voltage of the circuit is  $V_{CC} = 25$  V, the parameters of other electrical elements are  $C_0 = 50$  pf,  $R_0 = 100$   $\Omega$ ,  $R_1 = 1$  k $\Omega$ , and  $RL = 50$   $\Omega$ .

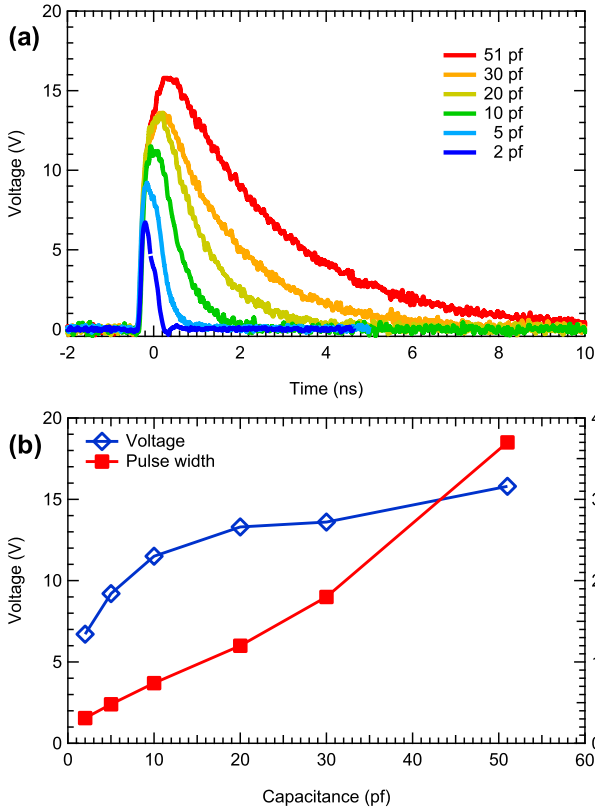


Fig. 3. (a) Waveforms of the electrical pulses with different storage capacitors. (b) Peak voltage and pulse width of the electrical pulses.

Fig. 3(a) shows the waveforms of the electrical pulses from the single avalanche-transistor-based circuit with different values of the storage capacitor  $C1$ . We observed that  $C1$  has a significant effect on the voltage and pulse width of the output electrical pulses. Fig. 3(b) summarizes the capacitance dependence of the peak voltage and pulse width of the electrical pulses generated from the generator. We observed that the output pulse voltage increases as capacitor  $C1$  increases, with the pulse width simultaneously increasing. The fall time of the output pulse is dominated by the discharging time  $\tau_2$  of the capacitor  $C1$  given by

$$\tau_2 = (r_E + R_L) \times C_1 \quad (3)$$

Here,  $r_E$  is the equivalent source impedance of the transistor circuit. Therefore, the output voltage and pulse width are two comprehensive factors that should be considered in choosing the volume of the storage capacitor.

Fig. 4 shows the circuit schematic of a designed Marx pulse generator consisting of 5 avalanche transistors. The working principle of the Marx generator is very similar to the single avalanche-transistor-based circuit in Fig. 2. Without the trigger signal, all the transistors in the circuit are turned off, the power supply voltage  $V_{CC}$  is charged to each capacitor  $C1-C5$ , and the voltages across the capacitors are close to the power supply voltage  $V_{CC}$ . In this condition, all the transistors are in a critical avalanche state. Once the trigger signal generated from an oscillator reaches the base of transistor  $Q1$ ,  $Q1$  will

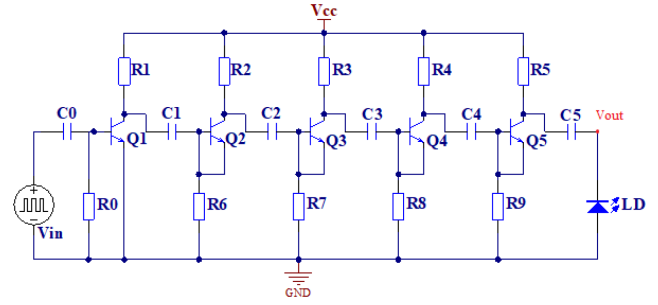


Fig. 4. Circuit schematic of the avalanche-transistor-based pulse generator.

experience avalanche breakdown immediately, and capacitor  $C1$  will be rapidly discharged. In an ideal condition, the left end of capacitor  $C1$  is instantly grounded, and the potential on the right end of capacitor  $C1$ , also the base of  $Q2$ , becomes  $-V_{CC}$ , and then transistor  $Q2$  will experience avalanche breakdown, consequently capacitor  $C2$  discharges rapidly through transistor  $Q2$ , and the potential on the right end of capacitor  $C2$  changes from zero to  $-2V_{CC}$ . Similarly, with the avalanche conduction of transistors  $Q3$ ,  $Q4$ , and  $Q5$ , the right end of the last storage capacitor  $C5$  (output side), will have a negative output pulse with a  $-5V_{CC}$  peak voltage in an ideal condition.

In fact, we constructed an electrical pulse generator, which is triggered by a common oscillator with a frequency of 4 MHz and a  $V_{CC}$  of 5 V. The applied DC voltage  $V_{CC}$  of the avalanche transistors is 25 V. An SMA interface is used for the output of the electrical pulses. Since the avalanche transistor produces negative pulses, the laser needs to be inverted, as shown in Fig. 4. And in this article, all the negative voltages have been made positive for ease of handling. In subsequent experiments that require voltage bias,  $V_{out}$  needs to be connected to the RF port of the biasT component, the DC bias needs to be connected to the DC port, and finally the output port needs to be connected to the laser diode.

A high-speed oscilloscope (Agilent 86100D) was used for the waveform measurements of the electrical pulses, where part of the signal from the oscillator on the PCB is used to trigger the oscilloscope. Fig. 5(a) shows two waveforms of the electrical pulses with different load impedances of 50  $\Omega$  and 5  $\Omega$ . We observed that the peak voltage and the pulse duration of the electrical pulses depend on the load impedance applied on the output of the pulse generator. With a load impedance of 50  $\Omega$ , the peak voltage is approximately 25 V with a duration of approximately 1 ns. While with a load impedance of 5  $\Omega$ , the pulse width can be as short as 0.45 ns with a reduced peak voltage of approximately 16 V. The mean jitter of the electrical pulses is measured to be only approximately 18 ps, indicating a very stable signal.

Fig. 5(b) shows waveform period of the electrical pulses, where the delta-function shaped pulses with a period of 250 ns are clearly demonstrated. The frequency of the output pulses depends on the used oscillator in the circuit, and can be changed by changing the clock frequency of the oscillator. Fig. 6 shows the output voltages of the Marx pulse generator with different

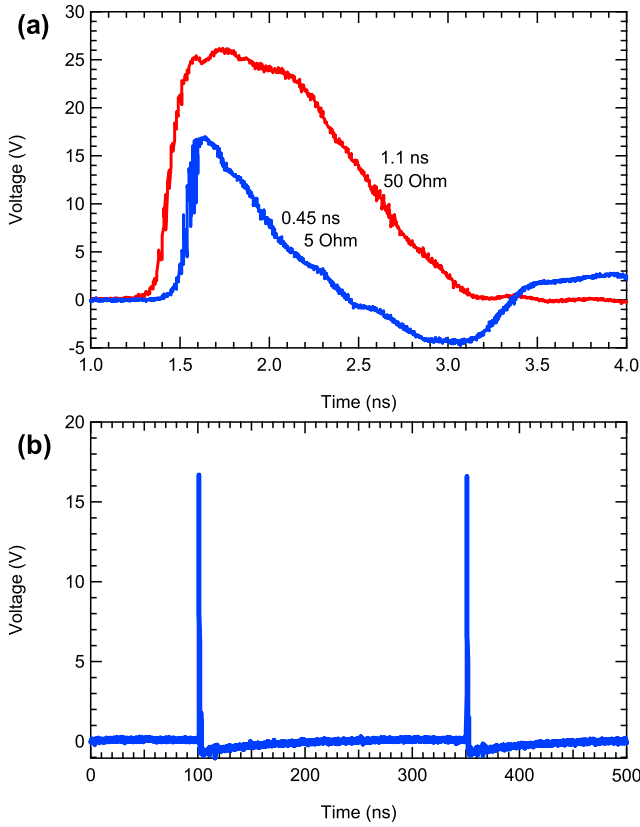


Fig. 5. (a) Waveforms of the electrical pulses with impedances of 50  $\Omega$  and 5  $\Omega$ . (b) Waveform period of the electrical pulses with a load impedance of 5  $\Omega$ .

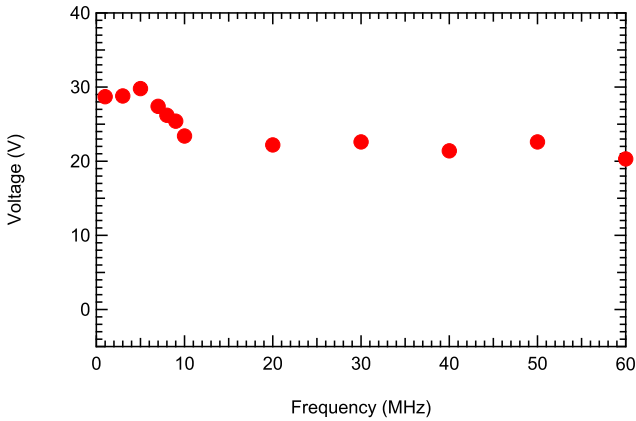


Fig. 6. Output voltage of the Marx pulse generator with different operation frequencies.

operation frequencies. The decrease in the voltage at high frequencies is considered to be caused by the insufficient charging of the capacitors at high operation frequencies.

During pulse generation, all the capacitors and the transistors in the 5-stage Marx generator ( $n = 5$ ) are connected in series. Following (3), the fall time of the output pulse is dominated by the time constant  $\tau_E$  given as

$$\tau_E = (R_E + R_L) \times C_E = (r_E \times n + R_L) \times C_1/n \quad (4)$$

Therefore, the effect of load impedance on the pulse width as demonstrated in Fig. 5(a) can be well understood. We used the same transistor and the same capacitor for each stage in the present generator. However, if there are some mismatches between the stages, their effects on the output pulses will be reflected through the equivalent resistance  $R_E$  and capacitance  $C_E$ . The non-uniformity of the switching time of the transistors will also affect the rise time of the output pulses. These effects should be considered during the design and optimization of the generators.

The output voltage of the circuit is much less than the maximum  $5V_{CC}$ , which can be attributed to the non-ideality of the electronic components, where the resistances in the transistors and the capacitors cannot be ignored because they can significantly reduce the output voltage. The maximum amplitude  $V_{MAX}$  of the output pulses can be given by

$$V_{MAX} = nU_0 \times R_L / (R_E + R_L) \quad (5)$$

Where  $U_0$  is the initial voltage across each capacitor before discharge. In order to get higher output voltage, one should try to measure the accurate equivalent impedance  $R_E$  of the circuit, and then choose proper load resistance to match the source impedance. Actually, a pulse generator capable of generating an output voltage of 15–25 V is sufficient for many practical applications, such as Electrical Time Domain Reflectometry (ETDR), which works by propagating an electrical pulse signal from one end of a transmission line and then monitoring the characteristics of each reflected pulse [16]. In particular, such pulse generator is very suitable for driving semiconductor laser diodes under gain-switching operation.

### III. PICOSECOND GAIN-SWITCHING OPERATION OF BLUE LASER DIODES WITH MARX GENERATORS

A GaN blue-violet single-mode laser diode with a pigtail package was used for this study. Compared to 1300 nm and 1550 nm lasers, 405 nm lasers have a higher forbidden bandwidth and require a higher voltage, which make it more difficult to excite. If a 405 nm laser can be successfully excited by our driver, those lasers with a longer-wavelength can certainly be excited. The continuous-wave (CW) lasing properties of the laser diode were first investigated with a DC current–voltage source (R6240A, Advantest) and a power meter (Q8230, Advantest). Fig. 7 shows the output power (right) and voltage (left) of the laser diode with different injection currents. The threshold voltage is 4.8 V and the threshold current is approximately 22 mA. From the light–voltage–current (L–I–V) curves of the laser diode, the slop efficiency is known to be approximately 0.55 W/A, and the resistance of the laser diode can be roughly estimated to be approximately 10  $\Omega$ . The inset shows that the lasing wavelength is approximately 405 nm, with a spectral width of 1.5 nm.

The GaN blue-violet laser diode was then used for optical pulse generation with the 5-avalanche-transistors-based Marx generator. The laser diode was connected to the electrical pulse generator through a simple connecting socket on the PCB for gain-switching characterizations, and the output of the electrical



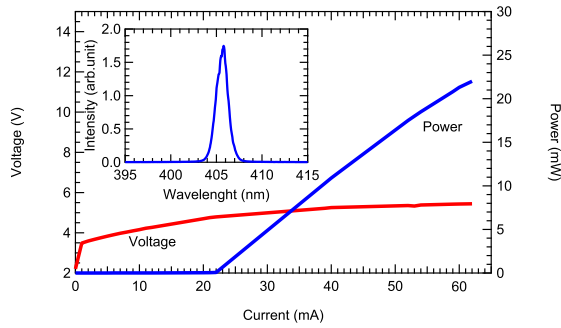


Fig. 7. Output power (right) and voltage (left) against injection current of the GaN laser diode. Inset shows a lasing spectrum of the laser diode.

pulse generator was connected to one channel of the high-speed oscilloscope simultaneously. Therefore, the equivalent load impedance of the circuit can be roughly estimated to be approximately  $8 \Omega$ , considering the  $50\text{-}\Omega$  equivalent impedance of the oscilloscope and the  $10\text{-}\Omega$  impedance of the laser diode. The optical signal from the laser diode was converted to an electrical signal through a high-speed photodetector (PD1004, Newport) with a response limitation of approximately  $12 \text{ ps}$ , and was subsequently measured through another channel of the high-speed oscilloscope.

Fig. 8(a) shows the synchronously measured waveforms of the electrical pulses applied on the laser diode and the output optical pulses from the laser diode. The initial times of the waveforms were adjusted according to the different lengths of the cables and the shapes of the falling edge of the electrical pulses. The measured pulse width of the electrical pulses is approximately  $0.8 \text{ ns}$ , and the voltage is approximately  $16 \text{ V}$ . The mean jitter of the electrical pulses is measured to be approximately  $20 \text{ ps}$ . The waveform of the optical pulses includes the first spike, the subsequent oscillation, and the steady-state component, which are typical characteristics of the pulses from gain-switched semiconductor lasers [17], [18]. The large contrast of the first spike to the steady-state component indicates the large gain of the laser diode, which is highly desired for short optical pulse generation.

Fig. 8(b) shows an enlarged waveform of the first spike of the optical pulse: the peak power is approximately  $550 \text{ mW}$ , the pulse width is measured to be approximately  $23 \text{ ps}$ , including a mean jitter of  $10 \text{ ps}$ . Namely, we successfully demonstrate a low-cost laser diode driver with a larger output power and narrower electrical pulses compared to the sub-ns pulse integrated CMOS driver chip [19]. By combining the driver with the laser, we obtain a simple laser seed source with only  $\sim 20 \text{ ps}$  pulse width. Most of the commercially available mature seed sources (e.g., Thorlabs, Photline & PicoQuant) have pulse widths of nearly  $100 \text{ picoseconds}$  and are very expensive. In contrast, ours is much more cheap and compact. Fig. 8(c) shows a log plot of the rising part of the waveform with a mono-exponential fitting. The constant rise time  $\tau_{rise} = 7 \text{ ps}$  obtained from the fitting result is a reflection of the saturation gain of the laser diode, which is a very important parameter that determines the gain-switching characteristics of the semiconductor laser diode [20],

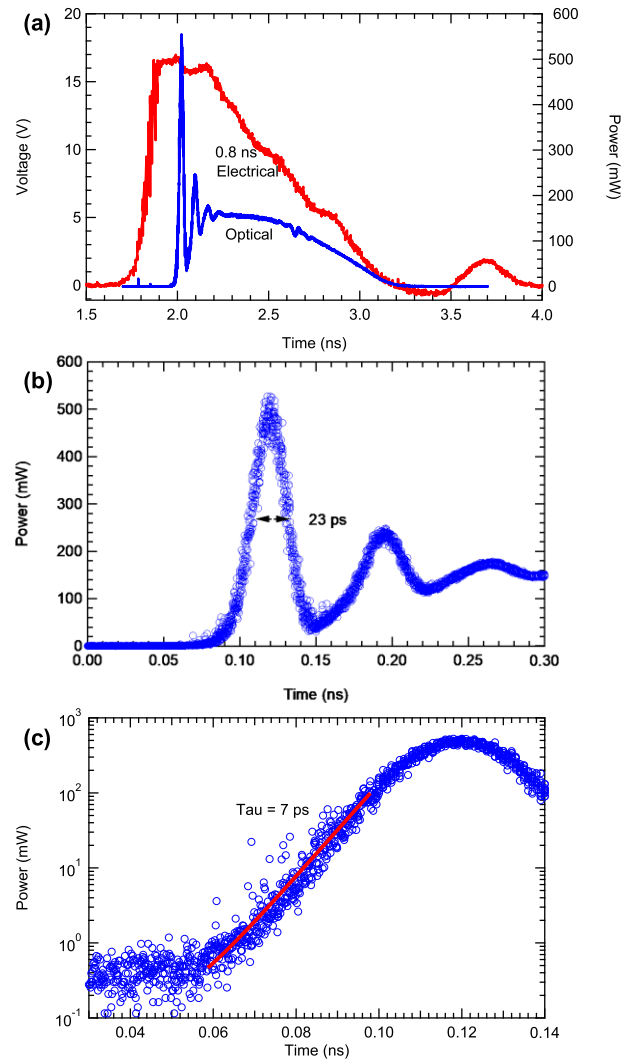


Fig. 8. (a) Waveforms of the electrical pulses applied on the laser diode and the optical pulses generated from the laser diode. (b) Enlarged waveform of the gain-switched optical output pulses from the laser diode, with a pulse width of  $23 \text{ ps}$  of the first spike of the pulses. (c) Log plot of the rise part of the waveform with a mono-exponential fitting (red solid line).

[21]. According to the relationship between the rise time and the saturation gain [21], and considering the general structure of the laser diode, the saturation gain of the present laser diode is estimated to be in the order of  $103 \text{ cm}^{-1}$ , which is still lower than the theoretical maximum values in literatures [22], indicating that the pulse width can be further reduced by optimizing the laser structures.

We tested the temporal stability and spectral stability of semiconductor lasers driven by Marx circuits, as shown in Fig. 9. The gain-switched semiconductor lasers can remain stable even without cooling devices such as thermoelectric coolers, and both the intensity and width have only a maximum fluctuation range of  $\pm 10\%$ . Consequently, it is reasonable to conclude that even if affected by the environment, the gain-switched semiconductor laser can continue to work stably to a certain extent. Without the effects of parasitic elements, the shape of the steady-state component of the gain-switched pulse should follow the waveform

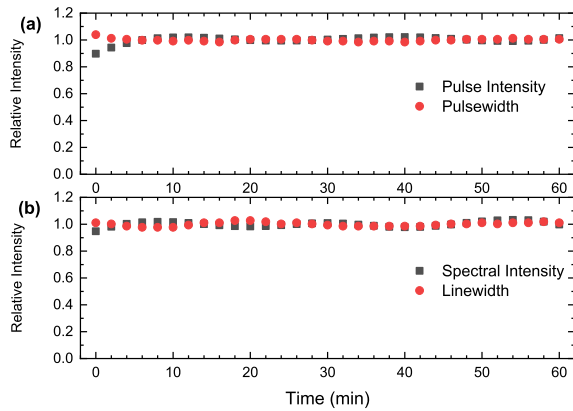


Fig. 9. Relative changes in the maximum value and width of the optical pulse (a) and the spectrum (b).

of the applied electrical pulses. The relative smooth waveform of the steady-state component of the optical pulse compared with the falling part of the electrical pulse indicates that the transient carrier density in the laser diode is not a direct reflection of the electrical pulse, but is modified by some additional effects such as the parasitic capacitance; consequently, even if some acupuncture signals exist in the electrical pulse, they may not affect the generation of optical pulses significantly. However, reducing the effects of parasitic capacitance in laser diodes remains necessary, especially for the case of using high-speed and ultrashort electrical pulses.

#### IV. FPGA-TRIGGERED MARX GENERATOR FOR STREAK-CAMERA CHARACTERIZATION

As demonstrated in Section III, the combination of a high-speed oscillator with a high-speed photodetector is very useful in measuring the waveform of the optical pulses from the gain-switched laser diode; however, this experimental setup cannot show the transient spectral characteristics, which are very important in understanding the gain-switching dynamics of semiconductor lasers.

A streak camera is a powerful tool that can measure the transient optical properties of gain-switched semiconductor laser diodes in both time- and wavelength-resolved methods. A streak camera has two major working modes: single shot mode and synchronous scan (synchroscan) mode. The synchroscan operation method of a streak camera has the advantages of high signal to noise ratio, and high-speed characterization. However, in the synchroscan model, the scanning repetition rate is strictly fixed at a certain value, for example 80 MHz, and the frequency of the signal must also be strictly synchronous with the scanning frequency of the streak camera. Commercially used programmable electrical pulse generator for generating electrical pulses with the required frequency to drive the semiconductor laser diodes for the gain-switching operation is very expensive and requires a large volume, which limit their practical applications in both industry and academia. Therefore, frequency-tunable low-cost electrical pulse generators are highly required.

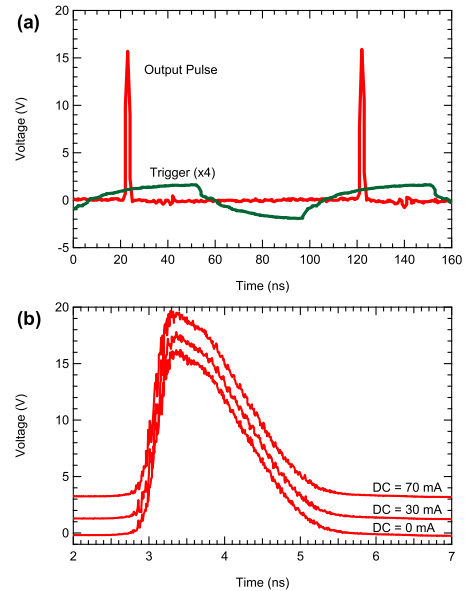


Fig. 10. (a) Waveforms of the electrical pulses Marx pulse generator, and the clock signals from the FPGA. (b) Enlarged waveforms of the pulses from the FPGA-triggered Marx generator with different bias currents of 0 mA, 30 mA, and 70 mA.

Here, we proposed a useful method to resolve this problem by the combination of a low-cost Marx generator and a low-cost FPGA (Field-Programmable Gate Array). An FPGA is widely used in many fields benefiting from its simplicity and programmability [23], [24]. It can be programmed to generate various signals with the required pattern and frequency, and can, therefore, be used to generate trigger signals with the required frequency for the avalanche-transistor-based Marx generator to generate electrical pulses for semiconductor laser diodes. The Marx generator used for this purpose was similar to the one shown in Fig. 4, where the oscillator generating clock signals was replaced with an FPGA.

Fig. 10(a) shows the clock signals from an FPGA, and the waveforms of the electrical pulses from the Marx pulse generator. As shown in Fig. 10(a), the frequency of the output pulse from the Marx generator is programmed with an FPGA to be 10.1 MHz, which is one eighth of the basic scanning repetition ratio of the streak camera (C10910, Hamamatsu), i.e., 80.85 MHz, and can be used for the synchroscan operation method.

A lab-made GaN laser diode with a can-type package was used for this demonstration. The fabrication procedure and the structure of the laser diode were given in a previous study [2]. Compared with single-mode lasers, lab-made multi-mode lasers have short high-energy pulses and long-lasting low-energy pulses when excited by long pulses. Single-mode laser diodes, on the other hand, can only produce pulses of a single wavelength. Otherwise, the performance of the two lasers is quite similar. The laser diode has a 160-mA continuous-wave lasing threshold. The lasing wavelength is approximately 450 nm. The laser diode was driven by the Marx generator with a DC bias. Fig. 10(b) shows the enlarged waveforms of the pulses from the FPGA-triggered Marx generator with different bias currents of 0 mA, 30 mA,

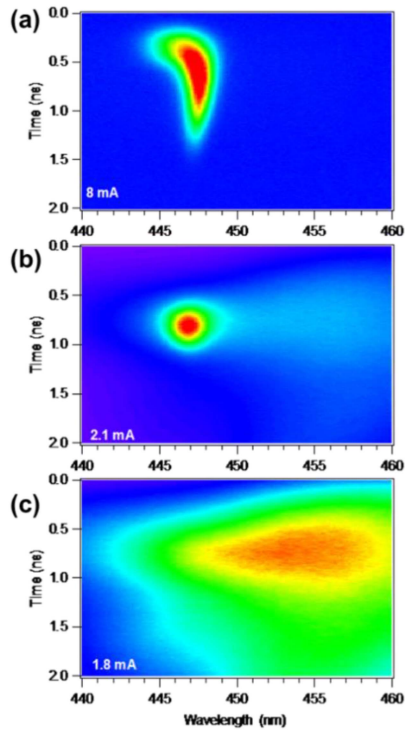


Fig. 11. Streak-camera images of the emission from the laser diode with different bias currents of (a) 8 mA, (b) 2.1 mA, and (c) 1.8 mA, respectively.

and 70 mA. As shown, with the DC current increased to 70 mA, the steady electrical level of the pulses was increased by 3.44 V, indicating that the resistance of the laser diode is approximately 50  $\Omega$ .

The electrical pulses generated from the Marx generator was applied on the GaN laser diode, and the signal from the FPGA was also used to trigger the streak camera. The lasing emission from the laser diode was collimated by an objective lens and was collected to the streak camera measurement system. Fig. 11 shows the measured time- and wavelength-resolved emission spectra of the laser diode with the streak camera. The spectral dynamics of the laser diode below and above the lasing threshold are clearly demonstrated. At below the threshold (1.8 mA), the streak camera image shows a spontaneous emission with a broad spectrum and a long duration of the laser diode. At the threshold (the DC bias threshold is 2.1 mA under fixed pulse excitation), the lasing emission appears at the short wavelength side of the spontaneous emission, and both the spectral width and pulse width of the emission were significantly decreased. The pulse width is measured to be approximately 430 ps. With an injection current of 8 mA, the image shows a very different pattern compared to the one around the threshold, where the pulse width shows a clear wavelength dependence.

Fig. 12 shows the spectra with different times of the gain-switched pulses extracted from the streak camera image. At the initial stage of the gain-switched pulse, the spectra are very broad with a full width at half maximum (FWHM) value of 2 nm. As time progresses, the spectra become narrower and shift to the long wavelength side. Fig. 13 shows the extracted waveform from the streak camera image. The total pulse width is measured

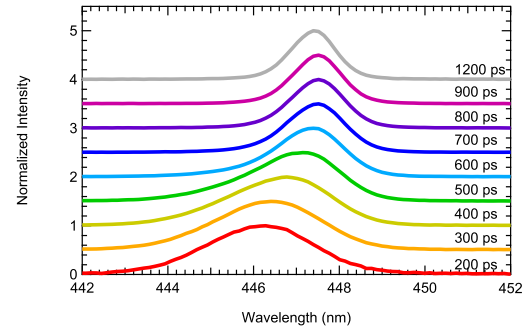


Fig. 12. Spectra with different pulse times extracted from the measured streak camera image of the laser diode with 8-mA injection current.

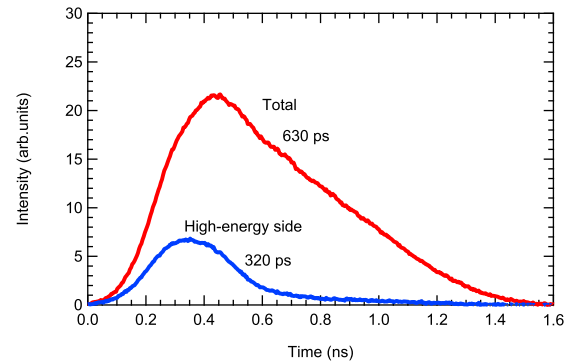


Fig. 13. Waveform of the pulses extracted from the measured streak camera image of the laser diode with 8-mA injection current.

to be approximately 630 ps, while the short wavelength side (high-energy side, < 446 nm) has a pulse width of approximately 320 ps. The characteristics of the wavelength-dependent pulse width of the gain-switched pulses was previously observed from single-mode semiconductor lasers [25], [26], and was attributed to the transient change in carrier density, which resulted in the index change. These results observed in the present study demonstrated that the characteristics of the wavelength-dependent pulse width also appears in the multiple-mode semiconductor laser; however, understanding the fundamental physics of these characteristics in multimode semiconductor lasers is still needed. The clear images of the gain-switched pulses taken with the streak camera demonstrated the practicability of the FPGA-triggered Marx pulse generator for characterizing the gain-switching properties of the laser diode with the low-cost current injection method, indicating the great potential applications of the Marx generators in the measurements of the time-resolved spectra of current-injected luminescence devices such as LEDs and laser diodes.

## V. CONCLUSION

We presented a low-cost subnanosecond electrical pulse generator based on avalanche transistors, where the output electrical pulses have a maximum peak voltage of 25 V and a minimum pulse width of 450 ps, depending on the output load impedance. We applied the electrical pulse generator on a GaN-based blue-violet semiconductor laser diode for the

demonstration of optical pulse generation via the gain-switching method; thus, optical pulses with a duration as short as 23 ps were obtained. These results demonstrated that even with the present avalanche-transistor-based low-cost electrical pulse generator, picosecond-short optical pulses from semiconductor lasers can be obtained via the gain-switching method. Such picosecond optical pulses can be used in TOF technique-based measurements to obtain higher signal-to-noise ratio and timing accuracy, i.e., higher measurement precision. In addition, we constructed an FPGA-triggered Marx generator with programmable frequency, and demonstrated the practicability of the characterization of the transient gain-switching properties of laser diodes with a streak camera. These results should be of significant interest for both industrial applications and scientific research.

#### REFERENCES

- [1] S. Q. Chen, A. Sato, T. Ito, M. Yoshita, H. Akiyama, and H. Yokoyama, "Sub-5-ps optical pulse generation from a 1.55- $\mu\text{m}$  distributed-feedback laser diode with nanosecond electric pulse excitation and spectral filtering," *Opt. Exp.*, vol. 20, no. 22, pp. 24843–24849, Oct. 2012, doi: [10.1364/oe.20.024843](https://doi.org/10.1364/oe.20.024843).
- [2] S. Q. Chen et al., "Picosecond tunable gain-switched blue pulses from GaN laser diodes with nanosecond current injections," *Opt. Exp.*, vol. 25, no. 12, pp. 13046–13054, Jun. 2017, doi: [10.1364/oe.25.013046](https://doi.org/10.1364/oe.25.013046).
- [3] J. L. Moll, "Avalanche transistors as fast pulse generators," *Proc. IEE-Part B: Electron. Commun. Eng.*, vol. 17, no. 106, pp. 1082–1084, 1959.
- [4] P. R. Prince, "Paralleling avalanche transistors," *Proc. IEEE*, vol. 53, no. 3, pp. 304–304, Mar. 1965.
- [5] S. N. Vainshtein, V. S. Yuferev, and J. T. Kostamovaara, "Properties of the transient of avalanche transistor switching at extreme current densities," *IEEE Trans. Electron Devices*, vol. 49, no. 1, pp. 142–149, Jan. 2002, doi: [10.1109/16.974761](https://doi.org/10.1109/16.974761).
- [6] S. N. Vainshtein, G. Duan, A. V. Filimonov, and J. T. Kostamovaara, "Switching mechanisms triggered by a collector voltage ramp in avalanche transistors with short-connected base and emitter," *IEEE Trans. Electron Devices*, vol. 63, no. 8, pp. 3044–3048, Aug. 2016, doi: [10.1109/ted.2016.2581320](https://doi.org/10.1109/ted.2016.2581320).
- [7] G. Duan, S. N. Vainshtein, and J. T. Kostamovaara, "Modified high-power nanosecond marx generator prevents destructive current filamentation," *IEEE Trans. Power Electron.*, vol. 32, no. 10, pp. 7845–7850, Oct. 2017, doi: [10.1109/tpel.2016.2632974](https://doi.org/10.1109/tpel.2016.2632974).
- [8] J. T. Li et al., "Theoretical analysis and experimental study on an avalanche transistor-based marx generator," *IEEE Trans. Plasma Sci.*, vol. 43, no. 10, pp. 3399–3405, Oct. 2015, doi: [10.1109/tps.2015.2436373](https://doi.org/10.1109/tps.2015.2436373).
- [9] H. M. Rein and M. Zahn, "Subnanosecond-pulse generator with variable pulsewidth using avalanche transistors," *Electron. Lett.*, vol. 11, no. 1, pp. 21–23, 1975, doi: [10.1049/el:19750016](https://doi.org/10.1049/el:19750016).
- [10] V. N. Rai, M. Shukla, and R. K. Khardekar, "A transistorized Marx bank circuit providing sub-nanosecond high-voltage pulses," *Meas. Sci. Technol.*, vol. 5, no. 4, pp. 447–449, Apr. 1994, doi: [10.1088/0957-0233/5/4/020](https://doi.org/10.1088/0957-0233/5/4/020).
- [11] Z. Y. Huang, Q. Fu, P. Z. Chen, H. C. Yang, and X. L. Yang, "High power pulse generator based on avalanche transistor Marx circuit," in *Proc. IEEE Int. Conf. Commun. Problem-Solving*, 2014, pp. 315–317.
- [12] P. Krishnaswamy, A. Kuthi, P. T. Vernier, and M. A. Gundersen, "Compact subnanosecond pulse generator using avalanche transistors for cell electroperturbation studies," *IEEE Trans. Dielectr. Electr. Insul.*, vol. 14, no. 4, pp. 871–877, Aug. 2007, doi: [10.1109/tdci.2007.4286518](https://doi.org/10.1109/tdci.2007.4286518).
- [13] Y. S. Gou et al., "High-speed, high-voltage pulse generation using avalanche transistor," *Rev. Sci. Instrum.*, vol. 87, no. 5, Jun. 2016, Art. no. 054708, doi: [10.1063/1.4948727](https://doi.org/10.1063/1.4948727).
- [14] J. Vanderwall, W. Hattery, and Z. Sztankay, "Subnanosecond rise time pulses from injection lasers," *IEEE J. Quantum Electron.*, vol. 10, no. 7, pp. 570–572, Jul. 1974, doi: [10.1109/jqe.1974.1068196](https://doi.org/10.1109/jqe.1974.1068196).
- [15] B. Lanz, S. Vainshtein, and J. Kostamovaara, "High power gain-switched laser diode using a superfast GaAs avalanche transistor for pumping," *Appl. Phys. Lett.*, vol. 89, no. 8, Aug. 2006, Art. no. 081122, doi: [10.1063/1.2337105](https://doi.org/10.1063/1.2337105).
- [16] S. J. Li, C. L. Chen, and K. J. Loh, "Laboratory evaluation of railroad crosslevel tilt sensing using electrical time domain reflectometry," *Sensors*, vol. 20, no. 16, Aug. 2020, Art. no. 4470, doi: [10.3390/s20164470](https://doi.org/10.3390/s20164470).
- [17] D. Bimberg, K. Ketterer, E. H. Bottcher, and E. Scholl, "Gain modulation of unbiased semiconductor lasers: Ultrashort light-pulse generation in the 0.8  $\mu\text{m}$ –1.3  $\mu\text{m}$  wavelength range," *Int. J. Electron.*, vol. 60, no. 1, pp. 23–45, Jan. 1986, doi: [10.1080/00207218608920760](https://doi.org/10.1080/00207218608920760).
- [18] K. Y. Lau, "Gain switching of semiconductor injection lasers," *Appl. Phys. Lett.*, vol. 52, no. 4, pp. 257–259, 1988, doi: [10.1063/1.99486](https://doi.org/10.1063/1.99486).
- [19] S. Rigault, N. Moeneclaey, L. Labrak, and I. O'Connor, "A low-voltage sub-ns pulse integrated CMOS laser diode driver for SPAD-based time-of-flight rangefinding in mobile applications," in *Proc. IEEE 32nd Int. Syst.-Chip Conf.*, 2019, pp. 5–10, doi: [10.1109/socce46988.2019.1570548090](https://doi.org/10.1109/socce46988.2019.1570548090).
- [20] T. Ito et al., "Transient hot-carrier optical gain in a gain-switched semiconductor laser," *Appl. Phys. Lett.*, vol. 103, no. 8, Aug. 2013, Art. no. 054708, doi: [10.1063/1.4819161](https://doi.org/10.1063/1.4819161).
- [21] S. Q. Chen et al., "Transient gain analysis of gain-switched semiconductor lasers during pulse lasing," *Appl. Opt.*, vol. 54, no. 35, pp. 10438–10442, Dec. 2015, doi: [10.1364/ao.54.010438](https://doi.org/10.1364/ao.54.010438).
- [22] W. W. Chow and S. W. Koch, *Semiconductor-Laser fundamentals: Physics of the gain materials*. Berlin, Germany: Springer, 1999.
- [23] H. Sun, Q. Deng, X. Liu, Y. Shu, and Y. Ha, "An energy-efficient stream-based FPGA implementation of feature extraction algorithm for LiDAR point clouds with effective local-search," *IEEE Trans. Circuits Syst. I-Regular Papers*, vol. 70, no. 1, pp. 253–265, Jan. 2023, doi: [10.1109/tcsi.2022.3212075](https://doi.org/10.1109/tcsi.2022.3212075).
- [24] C.-T. Chiu et al., "Chaos LiDAR based RGB-D face classification system with embedded CNN accelerator on FPGAs," *IEEE Trans. Circuits Syst. I-Regular Papers*, vol. 69, no. 12, pp. 4847–4859, Dec. 2022, doi: [10.1109/tcsi.2022.3190430](https://doi.org/10.1109/tcsi.2022.3190430).
- [25] S. Q. Chen et al., "Spectral dynamics of picosecond gain-switched pulses from nitride-based vertical-cavity surface-emitting lasers," *Sci. Rep.*, vol. 4, Mar. 2014, Art. no. 4325, doi: [10.1038/srep04325](https://doi.org/10.1038/srep04325).
- [26] S. Q. Chen, M. Yoshita, A. Sato, T. Ito, H. Akiyama, and H. Yokoyama, "Dynamics of short-pulse generation via spectral filtering from intensely excited gain-switched 1.55- $\mu\text{m}$  distributed-feedback laser diodes," *Opt. Exp.*, vol. 21, no. 9, pp. 10597–10605, May 2013, doi: [10.1364/oe.21.010597](https://doi.org/10.1364/oe.21.010597).